

# Methods

## TLSLeAF: automatic leaf angle estimates from single-scan terrestrial laser scanning

Atticus E. L. Stovall<sup>1,2,3</sup> , Benjamin Masters<sup>3</sup>, Lola Fatoyinbo<sup>1</sup>  and Xi Yang<sup>3</sup> 

<sup>1</sup>Biospheric Sciences Lab, NASA Goddard Space Flight Center, Greenbelt, MD 20771, USA; <sup>2</sup>Department of Geographical Sciences, University of Maryland, College Park, MD 20742, USA;

<sup>3</sup>Department of Environmental Sciences, University of Virginia, Charlottesville, VA 22903, USA

Authors for correspondence:

Atticus E. L. Stovall

Email: atticus.e.stovall@NASA.gov

Xi Yang

Email: xiyang@virginia.edu

Received: 15 April 2021

Accepted: 4 June 2021

New Phytologist (2021)

doi: 10.1111/nph.17548

**Key words:** 3D, forest, leaf angle distribution (LAD), light detection and ranging (LiDAR), radiative transfer model, terrestrial laser scanning (TLS), trees.

### Summary

- Leaf angle distribution (LAD) in forest canopies affects estimates of leaf area, light interception, and global-scale photosynthesis, but is often simplified to a single theoretical value. Here, we present TLSLeAF (Terrestrial Laser Scanning Leaf Angle Function), an automated open-source method of deriving LADs from terrestrial laser scanning.
- TLSLeAF produces canopy-scale leaf angle and LADs by relying on gridded laser scanning data. The approach increases processing speed, improves angle estimates, and requires minimal user input. Key features are automation, leaf-wood classification, beta parameter output, and implementation in R to increase accessibility for the ecology community.
- TLSLeAF precisely estimates leaf angle with minimal distance effects on angular estimates while rapidly producing LADs on a consumer-grade machine. We challenge the popular spherical LAD assumption, showing sensitivity to ecosystem type in plant area index and foliage profile estimates that translate to *c.* 25% and *c.* 11% increases in canopy net photosynthesis (*c.* 25%) and solar-induced chlorophyll fluorescence (*c.* 11%).
- TLSLeAF can now be applied to the vast catalog of laser scanning data already available from ecosystems around the globe. The ease of use will enable widespread adoption of the method outside of remote-sensing experts, allowing greater accessibility for addressing ecological hypotheses and large-scale ecosystem modeling efforts.

### Introduction

Leaf angle is a key biophysical property of vegetated canopies integral to accurate radiative transfer modeling, light interception, and leaf energy balance. Plants adjust leaf angle to gain resources (i.e. light) or adapt to environmental changes (Darwin, 1881; Ehleringer & Forseth, 1980; Kao & Forseth, 1992). Leaf angle distribution (LAD) – the relative proportion of leaves positioned between 0° (horizontal) and 90° (vertical) throughout a canopy – is a key parameter determining model simulated optical signal (e.g. it is a highly sensitive parameter determining the magnitude of solar-induced chlorophyll (Chl) fluorescence emitted by plants; Verrelst *et al.*, 2015). Similarly, changing LADs in radiative transfer models can change net canopy photosynthesis by *c.* 60% (Myneni, 1986). Even though LAD is a critical parameter, it is usually considered at plant functional-type level and treated as fixed during the growing season. For example, in the Community Land Model v.5, leaf angle is treated as a single parameter  $X_L$  that is fixed for each plant functional type (Lawrence *et al.*, 2019). Similarly, in radiative transfer models, LADs have been fixed to a few limited types (e.g. spherical, erectophile, planophile) and are often assumed to be stationary (van

der Tol *et al.*, 2009). The lack of accurate representation of LAD in ecosystem models is directly linked to an absence of efficient and accurate means of measuring LAD in canopies of diverse ecosystem structure.

Terrestrial laser scanning (TLS) instruments are ground-based devices using light detection and ranging (LiDAR) to hemispherically measure distances with extremely high resolution (*c.* 10 000 measurements m<sup>-2</sup>), providing a means to automatically measure leaf surfaces and LADs. TLS has recently become the most cutting-edge instrument for capturing forest and tree structure in three dimensions (Disney, 2019; Calders *et al.*, 2020) with major advances in allometric equation development (Momo Takoudjou *et al.*, 2017; Stovall *et al.*, 2017, 2018; Lau *et al.*, 2019) and remote-sensing calibration (Stovall & Shugart, 2018; Disney *et al.*, 2019). TLS can successfully measure leaf angle with a range of approaches, including plane fitting (Hosoi & Omasa, 2015), grid triangulation (Bailey & Mahaffee, 2017), and full three-dimensional (3D) estimation of surface normals (Vicari *et al.*, 2019). Yet, the individual benefits of previously developed methods have yet to be condensed into a single open-source pipeline capable of accepting minimally processed TLS data and efficiently reproducing leaf-level inclination angles.

Here, we present the Terrestrial Laser Scanning Leaf Angle Function (TLSLEAF), an open-source algorithm for automatically calculating spatially explicit leaf angle and LADs from gridded (or 'structured') – raw scan information describing the azimuth and zenith angles of individual laser pulses – TLS data. The basis for this method is the calculation of surfaces from the gridded point cloud, providing rapid and accurate surface normal computation. The aim of this particular method is to enable broad applicability and rapid estimation of leaf angle from minimally processed TLS data, overcoming the computational challenges of other approaches. First, we provide an overview of each major processing step in the TLSLEAF algorithm. Then, we validate our algorithm based on a laboratory experiment and data generated with a virtual forest. We conclude by applying TLSLEAF on five single scans from example sites of diverse forest structure, covering forests of managed loblolly pine (Colorado, USA), hemlock (Massachusetts, USA), temperate broadleaf (Virginia, USA), tropical broadleaf (Sarapiquí, Costa Rica), and mangrove (Libreville, Gabon). At these sites, we compare the impact of leaf angle on different approaches for estimating plant area index (PAI) and vertical foliage profiles. Finally, we apply these foliage profiles in a radiative transfer model, quantifying impacts on estimates of canopy net photosynthesis, absorbed photosynthetically active radiation, and solar-induced Chl fluorescence.

## Materials and Methods

### TLSLEAF method

TLSLEAF has been developed to automatically estimate LADs from gridded laser scanning data (Fig. 1). The open-access source code can be found at [github.com/aestovall/TLSLEAF](https://github.com/aestovall/TLSLEAF) (for permanent DOI, see the following Figshare link: <https://figshare.com/s/f2f0366d47529b8d9fd6>). To maximize accessibility, the algorithm is implemented in R (R Core Team, 2019) and relies heavily on the open-source CLOUDCOMPARE command-line tools (CloudCompare, 2020). Fig. 1 illustrates the main processing steps from a gridded single TLS scan to leaf angle estimates. The main processing steps for TLSLEAF involve the following: (1) rapid normal and angle estimates directly from the gridded TLS data; (2) leaf classification from a random forest classifier; and (3) voxel gridding and density correction. A description of the required user inputs and default values are detailed in Table 1. See Supporting Information Notes S1 for a short discussion of TLS acquisition considerations. For each scan, the algorithm produces a spatially explicit 3D voxel grid of average leaf angle and density-corrected LADs.

**Gridded terrestrial laser-scanning data** TLSLEAF primarily relies on gridded TLS data. Like hemispherical photography, from the perspective of the TLS instrument, pixels within a scan grid fully capture presence and absence of vegetation across the observed hemispherical area, while estimating the distance from the sensor. Much like other raster data, the spherically projected grid of distances can be directly gridded, creating pixel-based

estimates of surface properties. Before analysis, TLS data should be preprocessed and filtered (e.g. removing low-intensity returns), retaining only high-confidence range estimates. Once preprocessed, the only required input to the TLSLEAF algorithm is gridded TLS scan data (e.g. \*.ptx format or similar).

**Compute normals** TLSLEAF directly computes normal vectors ( $N \rightarrow$ , [ $N_x$ ,  $N_y$ ,  $N_z$ ]) from the gridded TLS data. Other approaches estimate leaf angle point-cloud normals in three dimensions (Vicari *et al.*, 2019), but normal orientation is widely known to be the most accurate and vastly more efficient (*c.* 3.9 million points (Mpts) per second in our tests) using gridded scan data, specifically due to the grid of continuous surface measurements from the scanner perspective (Badino *et al.*, 2011). In essence, surface normals of gridded TLS data can be directly computed using identical methodology to simple 2.5-dimensional raster analysis. Normals are computed at the pixel level with a moving  $3 \times 3$  grid, using the distances of points immediately adjacent to a focal pixel.

**Compute and filter by scattering angle** Scattering angle (the difference between the angle at which the laser pulse is reflected after intercepting an object in the scene and the normal vector of that surface) affects the accuracy of angle measurements and is used to filter anomalous leaf angle estimates. For instance, a beam traveling perpendicular to the surface normals of a leaf has a theoretical scattering angle of  $90^\circ$ , whereas a beam traveling parallel to the surface normals of a leaf has a scattering angle of  $0^\circ$ . Scattering angle is calculated using the following equation:

$$\alpha_{\text{scatter}} = \cos^{-1} \frac{\vec{N} \cdot \vec{xyz}}{|\vec{N}| |\vec{xyz}|} \times \frac{180}{\pi} \quad \text{Eqn 1}$$

where  $\vec{N}$ , the normal vector of the surface;  $\vec{xyz}$ , laser scanner beam vector. High scattering angles of  $\geq 80^\circ$  occur with anomalous leaf-edge measurements and tend to produce poor representations of surface normals. TLSLEAF computes and removes scattering angles  $> 85^\circ$  (Table 1; 'scatterLim').

**Compute leaf angle** TLSLEAF computes the angle of leaves and other visible surfaces relative to the horizon in the TLS scan grid directly from the surface normals. Surface angles are computed with:

$$\alpha_{\text{surface}} = \cos^{-1} \frac{\vec{N} \cdot \vec{z}}{|\vec{N}| |\vec{z}|} \times \frac{180}{\pi} \quad \text{Eqn 2}$$

where  $\vec{z}$ , the zenith vector. The inherent benefit of capturing incidence angle at the pixel level is that the algorithm captures leaf curvature, addressing the generally invalid assumption that leaf angle is a singular value. Rather, leaves display a diverse array of structures and curvature impacting the interception of light in the canopy environment. Thus, TLSLEAF estimates multiple angles per leaf. Other TLS-based algorithms rely on a similar

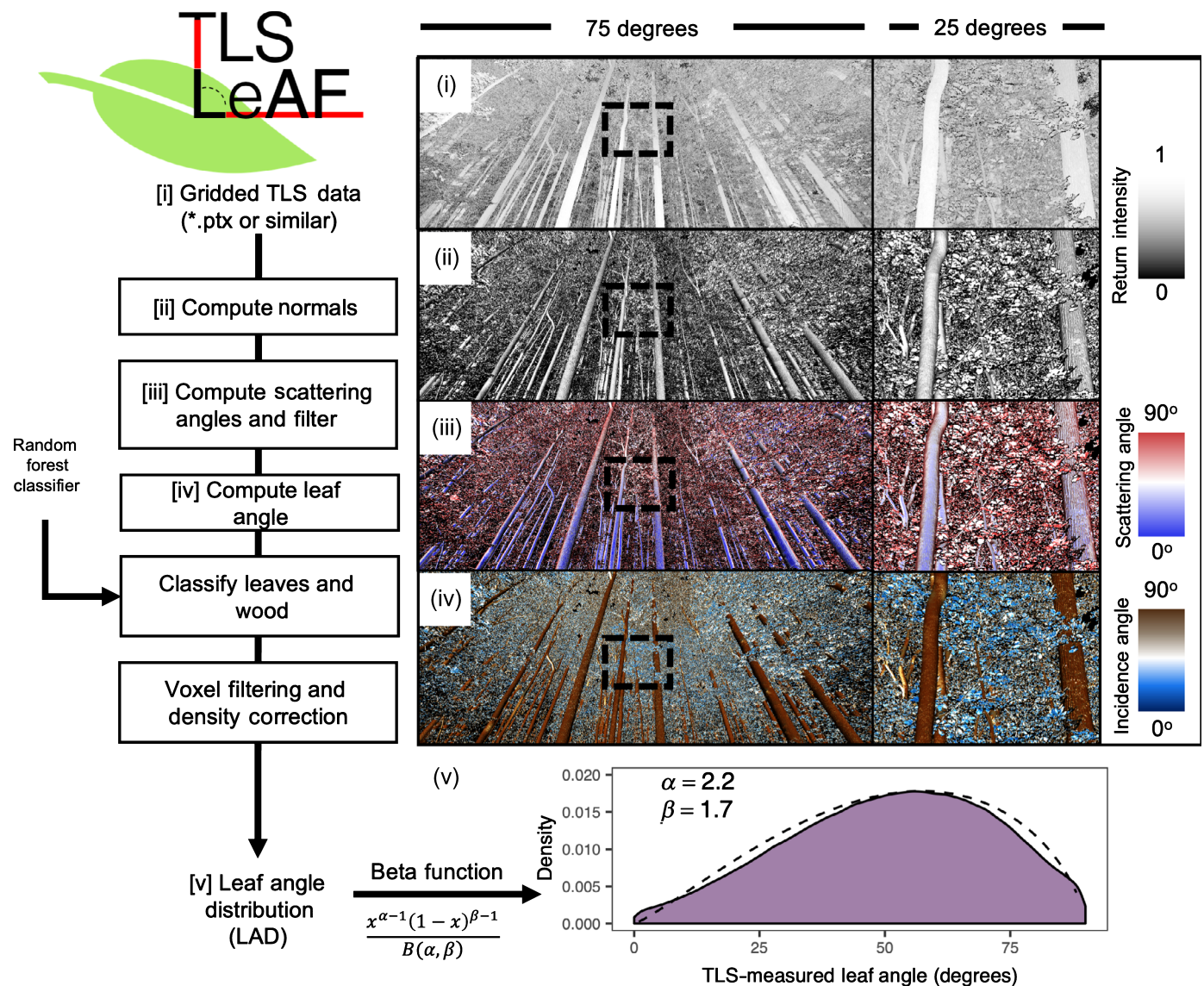


**Fig. 1** Overview of the processing pipeline implemented in TLSLeAF with visualization of each processing step on an example terrestrial laser scanning (TLS) scan of a mixed deciduous forest in Virginia, USA. Black dashed square shows zoom area in right panels. Note: The site depicted above was used to develop the random forest leaf classification, but excluded from the other site analyses.

processing framework but simplify pixel measurements into a single angular estimate (Bailey & Mahaffee, 2017). Instead, we approach modeling leaf angle at the measurement level (Vicari *et al.*, 2019), while gaining the benefits of more accurate angular estimates from gridded data.

**Classify wood and leaves** TLSLeAF differentiates leaf and wood surfaces with a supervised machine-learning (random forest) classifier relying on multiscale normal estimates (Krishna Moorthy *et al.*, 2019). We built a classified leaf–wood point cloud from temporally aligned data collected from leaf-off and leaf-on data (Fig. 2). We developed this approach specifically for broadleaf temperate forest since the leaf-off season enables high-confidence point-cloud classification – a method we believe will be useful in many other deciduous forest types. The point-cloud classification process involves the following steps: (1) fine-scale alignment of

the point clouds from two timesteps, (2) point-cloud distance computation, (3) leaf–wood differentiation based on distances 1 cm greater than the error in cloud coregistration (coregistration error 0.5 cm, distance threshold *c.* 1.5 cm). The resulting leaf-on point cloud (excluding the ground surface) is effectively and precisely classified as wood or leaf at a scale that is prohibitively time consuming using manual methods.

Next, we calculated surface normals from the 3D point cloud at three spatial scales (10, 50, and 75 cm), following Krishna Moorthy *et al.* (2019). Multiscale normal estimates are effective at differentiating objects with different structures (Brodu & Lague, 2012). In the case of leaf–wood differentiation, at the smallest scales, leaves appear to have planar surfaces, but normals become increasingly random with increasing spatial scale. Conversely, trunks and branch normals become increasingly linear. Each additional spatial scale at which normals are calculated adds three



**Table 1** Parameters for the R function, TLSLEAF.

| Variable      | Description  | Default value <sup>a</sup> | Units   |
|---------------|--|----------------------------|---------|
| input_file    | Path to gridded terrestrial laser scanning file (*.ptx or similar) | Required                   | —       |
| center        | Vector of scanner location in xyz coordinates.                     | Required                   | meters  |
| scatterLim    | Upper limit of scattering angle                                    | 85                         | degrees |
| SS            | Resolution of spatial subsampling procedure                        | 0.02                       | meters  |
| scales        | Spatial scales of normals for leaf–wood classifier                 | 0.1, 0.5, 0.75             | meters  |
| rf_model      | Random forest model for leaf–wood classification                   | Included                   | —       |
| voxRes        | Voxel size for density normalization                               | 0.1                        | meters  |
| minVoxDensity | Minimum measurements required per voxel                            | 5                          | —       |
| superDF       | Output results as object to environment                            | TRUE                       | —       |

<sup>a</sup>‘Required’ indicates user-specified values.

associated eigenvectors for which a classification can be based. In total, the random forest classifier using this approach is built from nine eigenvectors ( $N_x$ ,  $N_y$  and  $N_z$  at 10, 50 and 75 cm resolution). With this approach, we achieved accuracy (*c.* 88%) similar to Krishna Moorthy *et al.* (2019) with single-scan data and found, with visual inspection, the classifier was effective for most broadleaf forests tested. Spatial subsetting substantially reduced processing time (0.022 Mpts  $s^{-1}$ ) and had very little impact on classification accuracy. All training data and point clouds subject to processing with TLSLEAF are automatically subset to 2 cm spacing before the classification to decrease processing time.

**Voxel filtering** TLSLEAF normalizes leaf angle measurements at an optional voxel resolution approximately larger than the average leaf size (10 cm, by default; Fig. 3; Table 1, ‘voxRes’). Single-scan TLS data present a biased perspective of the forest canopy – decreasing measurements per unit volume as a function of distance from the scanner and vegetation density. As a result, LADs will be biased to the area closest to the TLS unit. TLSLEAF corrects this density measurement bias by, first, calculating statistics (mean and SD) of all angle measurements within voxels and, second, reconstructing the distribution of measurements within a voxel with an equal number of simulated angles. We exclude voxels with less than the first percentile of measurements across all voxels to further reduce anomalous measurements.

Before voxelization, an optional topographic normalization step can be included, detailed in Walter *et al.* (2021). In short, a ground surface model is reconstructed from the single-scan TLS data and subtracted from the vertical dimension of the TLS point cloud (Roussel *et al.*, 2020), effectively normalizing by topography – see Walter *et al.* (2021) for details. Topographic normalization was included in TLSLEAF to allow for vertical profiles of mean leaf angle and LAD, which can be reconstructed with a simple summary operation (e.g. aggregate) along the vertical dimension of the voxelized output.

**Estimate leaf angle distributions** The final processing stage of TLSLEAF uses the statistics derived at the voxel filtering stage to estimate the normalized LAD. Ten random samples are generated from a normal distribution with mean and SD of the voxel-level statistics calculated in the previous step. The processed voxels provide a spatially explicit distribution of leaf angle estimates

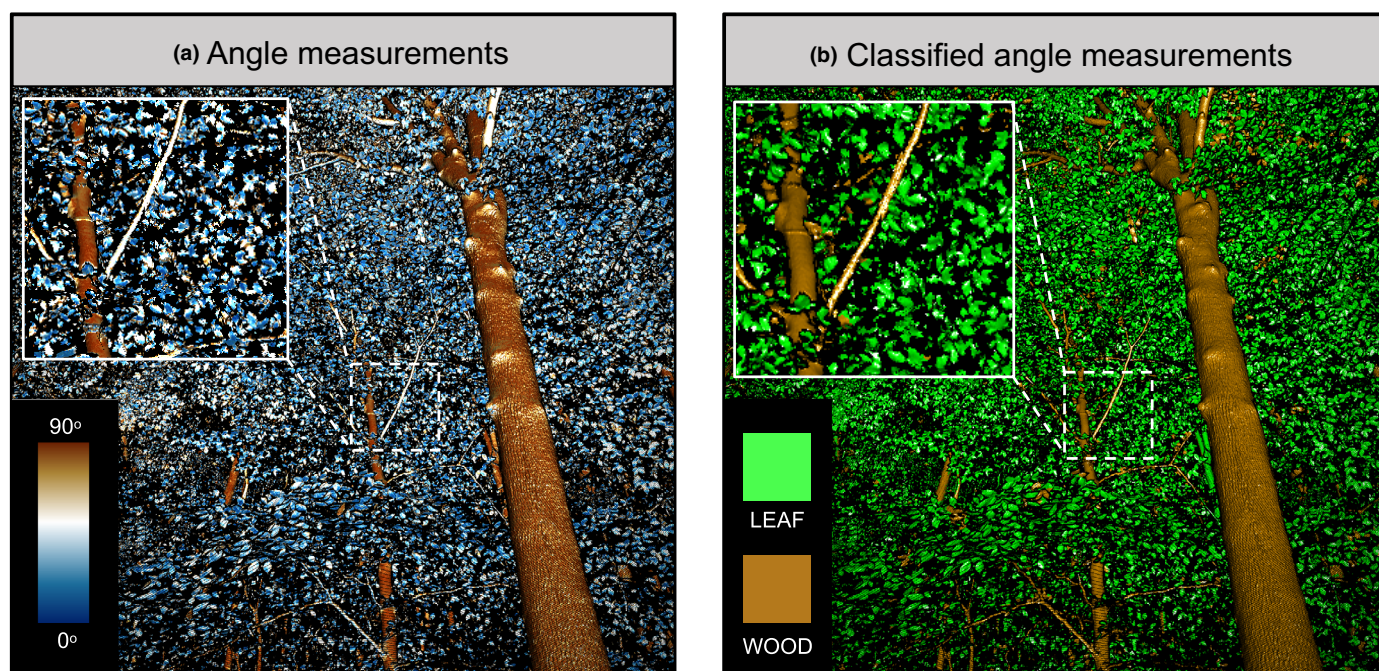


**Fig. 2** Single-scan random forest leaf–wood classification. (a) Angle estimates are classified into (b) leaf and wood measurements for accurate reconstruction of leaf angle distributions.



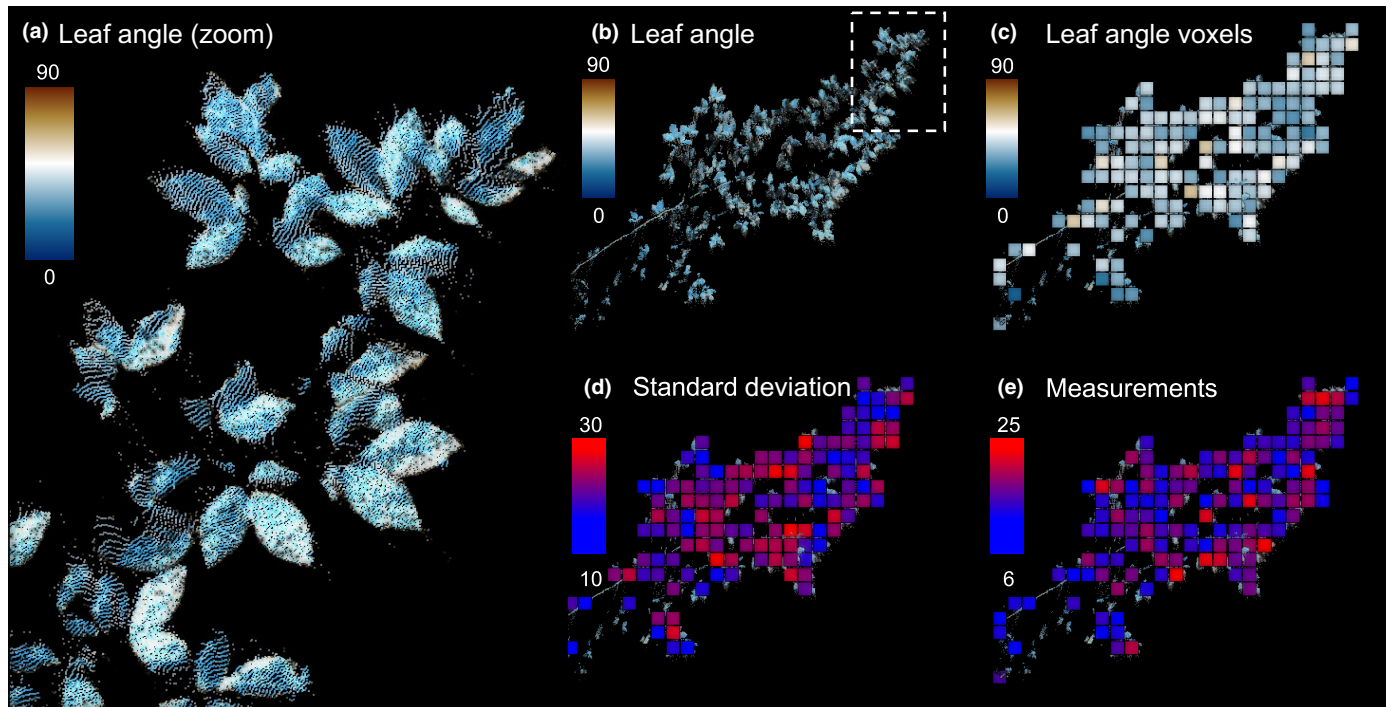


**Fig. 3** TLSLeAF voxelization process (nadir view angle) for normalizing angular measurements. (a, b) High-resolution leaf angle estimates (c. 5 m measurement distance shown) are voxelized at 10 cm resolution and (c) mean, (d) SD, and (e) number of measurements are derived for correcting leaf angle distributions.

at the defined voxel resolution. At this stage, the LAD Beta function parameters ( $\alpha$  and  $\beta$ ) can be estimated using:

$$\frac{x^{\alpha-1}(1-x)^{\beta-1}}{B(\alpha, \beta)} \quad \text{Eqn 3}$$

where  $B(\alpha, \beta) = (\Gamma(\alpha)\Gamma(\beta))/(\Gamma(\alpha + \beta))$ ;  $\Gamma$ , the gamma function. Such parameters can be used directly as input parameters in radiative transfer models.

**Derive  $G$ -function** The LAD derived from TLSLeAF can be used to directly calculate the  $G$ -function (mean leaf projection area). We used the following equation from Wilson (1960) to calculate the  $G$ -function:

$$G(\theta) = \int_{\theta_1=0}^{\pi/2} G(\theta, \theta_1) p(\theta_1) d\theta_1 \quad \text{Eqn 4}$$

where  $\theta_1$ , zenith angle of leaf normal;  $G(\theta, \theta_1)$ ,  $G$ -function with leaf zenith angle fixed at  $\theta_1$  and random leaf azimuth angle;  $p(\theta_1)$ , probability density function of leaf zenith angle. The probability density function is assumed to be randomly distributed throughout the canopy, yet spatial differences in leaf angle are widely observed (e.g. more horizontal leaf angle in understory to maximize light interception; Horn, 1971; Posada *et al.*, 2009; Givnish, 2020). As such, we also consider a formulation of the  $G$ -function that derives the probability density function at each solid angle bin  $\theta$  before integration. Using this method, we account for

different LADs with respect to view zenith angle, providing a more accurate representation of the mean leaf projection area function.

### Benchmarking TLSLeAF

We benchmarked each processing step of TLSLeAF on a consumer-grade laptop – a 2015 MacBook Pro (MacBookPro12,1) with a 3.1 GHz Intel Core i7 and 16 GB 1867 MHz DDR3 RAM. TLS processing primarily requires large RAM resources, but, at times, a faster CPU can be beneficial. We anticipated this machine would provide an upper limit of acceptable processing time typical for most users.

### Validating TLSLeAF

TLSLeAF was validated with a laboratory experiment using a Faro Focus 120 TLS unit and 19 plastic leaves (c. 5 cm × 15 cm dimensions) placed at approximately 5° intervals from 0 to 90° hand-measured with a leaf inclinometer. Note that the hand measurements only provide the leaf angle at the center of the leaf, which may not be representative in curved leaves. We used a laboratory-based experiment so we might capture uncertainty due to factors that are more difficult to simulate (e.g. edge ranging errors common on phase-shift TLS instruments). The TLS has a beam divergence of 0.19 mrad and collected 0.768 mrad resolution scans for a total 26 541 212 potential returns per scan (8258 × 3214 grid, azimuth × zenith). We focused specifically on how effective

TLSLEAF is at estimating leaf-level angles and reconstructing the LADs.

In comparison with hand-measured leaf angles, we evaluated the distribution of leaf angle estimates with respect to leaf distance. We assessed the effect of scanner distance by placing the TLS at 2, 5 and 10 m distance from the test leaves, applying the algorithm with the default parameters in each case. We also tested the effect of scattering angle on leaf angle measurement error. Finally, we directly compared the hand-measured (approximately uniform) and TLS-measured LADs, testing for significant differences using a Kolmogorov–Smirnov (KS) test.

Finally, we implemented a number of validation experiments in a virtual environment (Fig. S1; Notes S2) to test the effects of occlusion, scan angular resolution, and distance from target in single-tree and forest scenarios. See Notes S3 for an additional analysis addressing the sensitivity of leaf angle measurements to TLS parameters (Fig. S2) and voxel resolution (Fig. S3). We validated and assessed errors in LAD estimates with the known LAD of a realistic 3D 5 m tall broadleaf tree object. The 3D wood and leaf surfaces are composed of a digital mesh surface that is sampled along with surface angles at a resolution higher than captured with TLS instruments (*c.* 20 000 points  $\text{m}^{-2}$ , *c.* 37 Mpts per tree object). In the forest scenario, this single tree was duplicated and positioned with approximately even *c.* 2.5 m spacing, creating an even-aged closed canopy scenario, ideal for

assessing occlusion in different positions throughout the digital forest. For our tests, we simulated TLS data using two patterns (Fig. 4). In the single-tree scenario, we ran the simulation using a box pattern, positioned at four corner positions using intervals of 5, 10, 20, 30 and 60 m. For the forest scenario, we ran the simulation at nine different positions around and in the center of a 10 m  $\times$  10 m forest cloud. The range of positions in both scenarios allowed us to capture variation in the LAD due to occlusion – a major factor and consideration in a real forest environment. We also tested three TLS scanner resolutions in all positions of the single tree scenario tested:  $0.05^\circ$ ,  $0.025^\circ$  and  $0.01^\circ$ . In the forest scenario, we tested the coarsest resolution scan as an upper limit of our error expectations. The surface angle estimates from these simulations were then compared directly with the full tree or forest-level LAD.

### Applications of TLSLEAF in diverse forest types

As a simple demonstration, we applied the TLSLEAF algorithm with default settings to single scans from a diverse set of five sites chosen for their relatively divergent forest structure: the managed loblolly pine stand in Colorado, USA, which is part of the Colorado State Forest; the hemlock stand in Massachusetts, USA, which is part of Harvard Forest; the temperate broadleaf forest in Virginia, USA, and within the 40 m tall old-growth tulip poplar

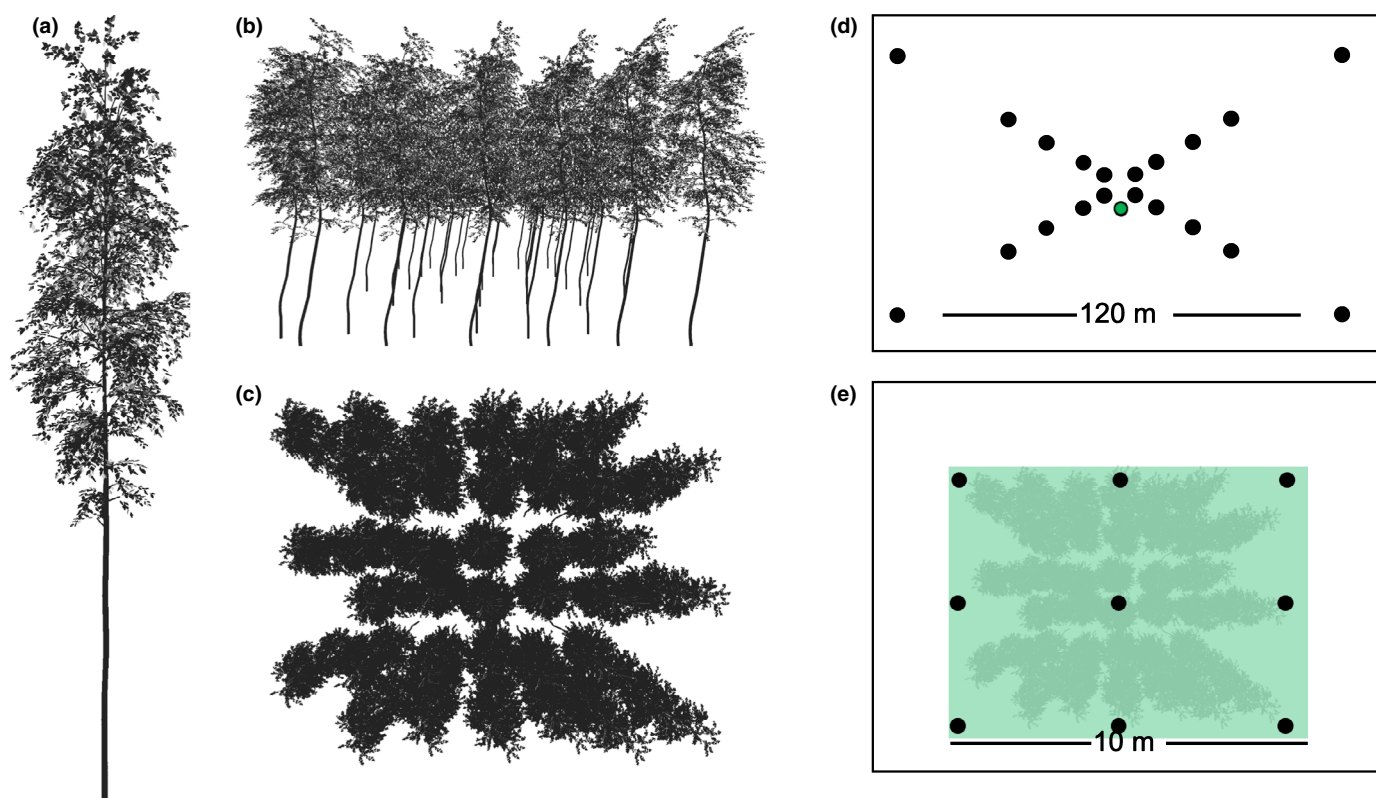


**Fig. 4** Simulated three-dimensional tree and simple forest environment used for the validation testing scan resolution, distance, and occlusion. (a) Side-view of the model tree used; (b) side view of the virtual forest; (c) top view of the virtual forest; (d) single-tree (green) simulation scan positions (black) ranging from 5 to 85 m distance at three different scan resolutions. (e) Nine scan positions (black) across the 10 m  $\times$  10 m simulated forest environment (green).



(*Liriodendron tulipifera*) forests of Montpellier; the tropical broadleaf forest in Sarapiquí, Costa Rica, which is a late-stage secondary stand with palm in the understory; and the mangrove forest, which is the tallest known stand, towering *c.* 60 m in height, located outside of Libreville, Gabon, in Pongara National Park. For each site, we derived LADs, vertical distributions of mean leaf angle, beta parameters, and the *G*-function for comparison in the context of foliage profiles and radiative transfer-model-based estimates of canopy fluxes.

We used the derived LADs and *G*-functions to evaluate the impact on estimates of PAI and plant area vegetation density (PAVD; vertical distributions of plant area) profiles across all five sites. PAI and PAVD are typically estimated using an array of methods derived from the gap fraction – the fraction of the canopy with ‘sky’ or ‘soil’ gaps, depending on view perspective. Jupp *et al.* (2008) detailed a method adapted for TLS from MacArthur & Horn (1969). The key equation describing vertically resolved gap fraction is:

$$P_{\text{gap}}(\bar{\theta}, z) = 1 - \frac{\sum_i^j (z_i < z, \bar{\theta})}{N(\bar{\theta})} \quad \text{Eqn 5}$$

where *z*, the height above ground;  $\bar{\theta}$ , the midpoint of the 5° zenith angle range used to aggregate TLS returns. This equation describes the cumulative number of returns per unit height divided by the total number of outgoing laser pulses *N*. In essence, intercepted vegetation progressively reduces the probability of a laser pulse escaping the canopy.

PAI and PAVD are typically estimated with  $P_{\text{gap}}$  at the hinge angle – a viewing zenith angle of 57.5°. The hinge angle is used to estimate total PAI, as this is the angle at which the canopy-level *G*-function is nearly invariable at 0.5 for all typical LADs (Jupp *et al.*, 2008). We approximate the hinge angle as the 5° zenith bin between 55° and 60°.  $P_{\text{gap}}$  is converted to the cumulative PAI profile using:

$$L(z) \approx -1.1 \log P_{\text{gap}}(57.5^\circ) \quad \text{Eqn 6}$$

The coefficient value of 1.1 is derived from the extinction coefficient  $k(57.5^\circ)$ , defined as  $\cos(57.5^\circ)/G(57.5^\circ)$ . The derivative of this cumulative profile provides a height-specific estimate of PAI, or PAVD. Since LAD is rarely known, profiles from each zenith angle bin are scaled to equal the PAI estimate from the hinge angle (Jupp *et al.*, 2008).

Jupp *et al.* (2008) also described a linear approximation method using the following equation:

$$L_h + L_v X(\theta) \approx -\log P_{\text{gap}}(\theta, z) \quad \text{Eqn 7}$$

$$X(\theta) = \frac{2}{\pi} \tan(\theta)$$

where  $L_h$  and  $L_v$ , horizontal and vertical components of PAI. Essentially, a linear model is fit between  $X(\theta)$  and  $-\log P_{\text{gap}}(\theta, z)$ , providing an estimate of cumulative leaf area with height or  $L(z)$  for which the derivative and PAVD profile can be determined.

With TLSLEAF, we capture both random and view-angle-specific LAD, allowing PAVD and PAI to be estimated with greater precision. A spatially random LAD assumes that the measured LAD is homogeneous throughout the canopy. A more realistic scenario considers LAD as nonrandom in the canopy, varying with respect to zenith angle and accounting for variation in angle due to differing light conditions (Horn, 1971; Givnish, 2020). The modification of Eqn 6 is as follows:

$$L(\theta, z) \approx -\frac{\cos(\theta)}{G(\theta)} \log P_{\text{gap}}(\theta) \quad \text{Eqn 8}$$

$L(\theta, z)$  is estimated for each zenith angle bin, instead of 57.5° only. After the derivative of this profile is computed, the distributions of PAVD in each zenith angle bin are aggregated and summarized in terms of mean and SD of the PAVD profile.

We compared four methods of estimating PAI and PAVD profiles. Method 1 relied solely on the hinge angle estimates described in Eqn 6. Since this method was derived at a single angular bin, SD values were not calculated. Method 2 used Eqn 8 and assumed LAD was randomly distributed. Method 3 also used Eqn 8 but relied on the actual LADs in each inclination angle bin. Our hypothesis is that this method is closest to the reality. Method 4 used the linear approximation described in Eqn 7. Since the hinge angle (method 1) is the most commonly used method of estimating PAI with TLS (and hemispherical photography), we used these estimates as a baseline for comparison, calculating absolute and percentage deviation for all other methods.

We used MSCOPE (Yang *et al.*, 2017) a multilayer one-dimensional radiative transfer, photosynthesis, and energy balance model to simulate the effect of using different profiles on the simulated fluxes, including canopy net photosynthesis (Actot,  $\mu\text{mol m}^{-2} \text{s}^{-1}$ ), absorbed photosynthetically active radiation (APAR,  $\mu\text{mol m}^{-2} \text{s}^{-1}$ ), and solar-induced Chl fluorescence (SIF; hemispherical top-of-canopy SIF,  $\text{W m}^{-2}$ ). SIF can be remotely sensed, and it is related to canopy photosynthesis (e.g. Frankenberg *et al.*, 2011; Yang *et al.*, 2015; Magney *et al.*, 2017). We used default model parameters (fixed incoming radiation at  $600 \text{ W m}^{-2}$ , air temperature at 20°C, maximum carboxylation rate at  $80 \mu\text{mol m}^{-2} \text{s}^{-1}$ ) except for the canopy leaf area index (LAI) profile and the total LAI. LAD was assumed to be spherical. Here, the primary goal was to evaluate the impact of different representations of PAI and PAVD on canopy fluxes, providing insight into the effects on remote sensing and ecological modeling. Note that MSCOPE does not take vertical LAD as an input, and thus we only investigate the impact of LAD indirectly through the vertical leaf area distribution.

## Results

### Benchmarking TLSLEAF

TLSLEAF rapidly processes single-scan TLS data in an R coding environment (Fig. 5). In our tests, one TLS scene with *c.* 26 Mpts requires *c.* 9 min for TLSLEAF to fully process the data. Breaking the method into steps, normal computation using

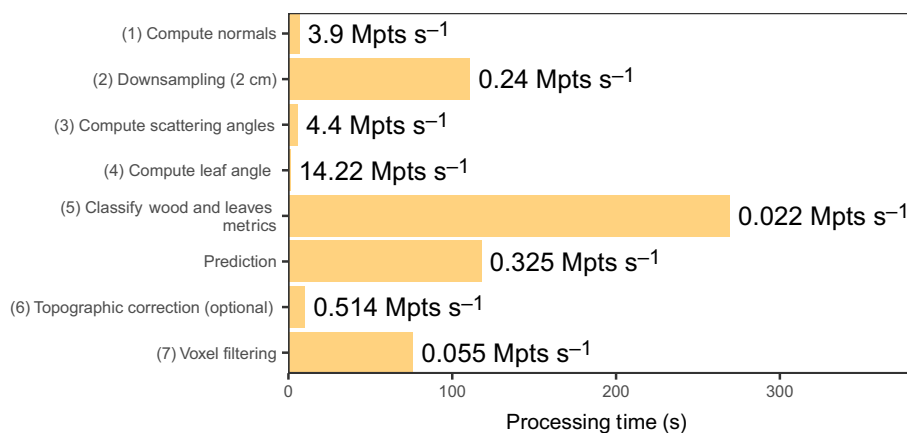


**Fig. 5** Overall processing time and speed of TLSLEAF method with an  $8258 \times 3214$  gridded terrestrial laser scanning scan. Leaf-wood classification is separated into the multiscale computation of normals and random forest prediction steps. Topographic correction is optional, depending on the desired output of the user.

gridded TLS scans was extremely rapid ( $3.9 \text{ Mpts s}^{-1}$ ) compared with full 3D octree-based normal computation, which failed to complete a single scan after 1 h of processing time. Downsampling required  $0.24 \text{ Mpts s}^{-1}$ , but, in testing, we found substantial downstream computational benefits by including this step. Steps relying on precomputed normals were extremely rapid – scattering angles were computed at  $4.4 \text{ Mpts s}^{-1}$ , and leaf angles were computed at a rate of  $14.22 \text{ Mpts s}^{-1}$ . Derivation of multiscale normals for leaf classification was the slowest process at a rate of  $0.022 \text{ Mpts s}^{-1}$ , but random forest classification was faster ( $0.325 \text{ Mpts s}^{-1}$ ). The optional topographic normalization step added minimal total time to processing, and the final voxel normalization was completed at a rate of  $0.055 \text{ Mpts s}^{-1}$ .

### Validating TLSLEAF

In  $\approx 85\%$  (16/19) of samples, the mode of the leaf-level angle distribution closely represented the hand-measured value irrespective of distance (Fig. 6). For leaf angles approximately perpendicular to the scanner view angle ( $< 20^\circ$ ) – or those with high scattering angles – less leaf-level measurements were captured, producing less-confident leaf angle estimates. Our validation against hand-measured angles had  $12.7^\circ$ ,  $14.5^\circ$  and  $18.2^\circ$  RMSE and  $0.1^\circ$ ,  $-1.8^\circ$  and  $2.1^\circ$  bias, for 2 m, 5 m and 10 m, respectively (Fig. 7). However, when using the 2 m TLS angular estimates as our validation data set, error was substantially lower (RMSE:  $3.9^\circ$  for 5 m;  $8.3^\circ$  for 10 m) and less biased (bias:  $-1.9^\circ$  for 5 m;  $-2.2^\circ$  for 10 m) (Fig. 7). TLSLEAF recreated statistically similar LADs to the manual measurements at 2 m, 5 m, and 10 m (KS test:  $P = 0.76$ ,  $P = 0.74$ ,  $P = 0.55$ , respectively; Fig. 7). Aggregated across all distances, the LAD remains representative of manual measurements (KS test:  $P = 0.75$ ). We compared the area-normalized 2 m TLS LAD with the 10 cm voxel aggregated approach (as is used in TLSLEAF) finding minimal differences between the shapes of the two distributions (5 m:  $R^2 = 0.98$ ; 10 m:  $R^2 = 0.99$ ; Fig. 7e).

The single-tree and forest simulation validations are consistent with the manual validation, showing distance increases errors in leaf angle estimates (Fig. 8). In the highest resolution scenario, RMSE increased with distance in the single-tree simulation, increasing from  $\approx 5^\circ$  at 5 m distance to  $\approx 9^\circ$  at 85 m. The

lowest resolution increased RMSE to  $9^\circ$  at 5 m distance and up to  $17^\circ$  at  $85^\circ$ . The variation within a single distance interval shows occlusion can account for a substantial portion of the measurement error ( $\approx 10^\circ$  in the 85 m low-resolution scenario). Distance tends to positively bias leaf angle measurements by a maximum of  $\approx 2^\circ$ . The variation in the LAD increases with lower resolution scans, but on average closely matches the true LAD. The simulated TLS scans from every position in the simulated forest closely matched the true LAD, with  $\approx 6^\circ$  average RMSE (ranging from  $4^\circ$  to  $8.9^\circ$ ) and  $\approx -0.2^\circ$  bias (ranging from  $-0.4^\circ$  to  $+0.1^\circ$ ).

### Applications of TLSLEAF in diverse forest types

When we apply TLSLEAF to TLS data collected in different types of forested ecosystems, we found substantial variations in parameters of beta function,  $G$ -function, and leaf angle profile. In each test case, a single gridded scan file was automatically processed and LADs were produced without additional user input (Fig. 9). The LAD of needleleaf systems peaked at higher leaf angles,  $\approx 90^\circ$ . The closed canopy of Harvard Forest had a sharp peak near  $90^\circ$  ( $\alpha = 2.0$ ,  $\beta = 0.9$ ), whereas the open managed loblolly pine forest had a peak near  $75^\circ$  ( $\alpha = 2.7$ ,  $\beta = 1.4$ ). The tallest, most open broadleaf systems had identical beta parameters ( $\alpha = 2.2$ ,  $\beta = 1.7$ ), with peaks near  $50^\circ$ . The broadleaf tropical forest was also similar, but peaked around  $60^\circ$  ( $\alpha = 2.3$ ,  $\beta = 1.8$ ).

We found the  $G$ -function to differ substantially in shape and magnitude, depending on how LAD was represented in the canopy (Fig. 9). The random LAD method resulted in a smooth LAD curve, whereas the nonrandom LAD method was more variable in shape. The random LAD assumption produced  $G$ -functions that were more spherical to erectophile in needleleaf systems (hemlock and pine dominant) and more planophile in broadleaf systems (temperate, tropical, and mangrove). The non-random assumption of LAD created  $G$ -functions that deviated substantially from the random assumption method. Since these more variable  $G$ -functions are unlike the theoretical functions, we are unable to clearly classify them into established categories.

Each site displayed a unique trend in the vertical distribution of mean leaf angle (Fig. 9). The open loblolly pine stand in



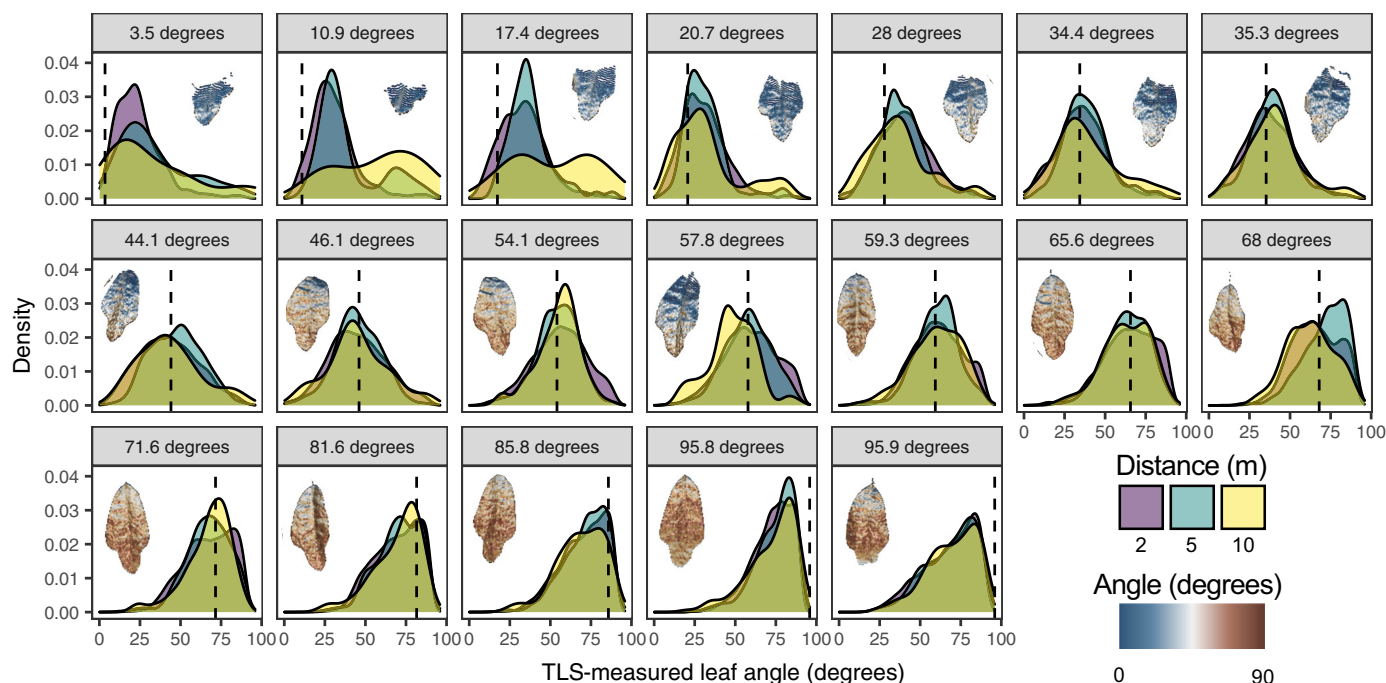


**Fig. 6** Leaf-level inclination angle distribution in comparison with manual measurements (vertical dotted line) at three distances. Terrestrial laser scanning (TLS) leaf-level angle measurements are overlaid on their respective distribution and color coded by angular estimate.

Colorado had little variability with height, averaging *c.* 50°. The hemlock stand at Harvard Forest had a consistent increase in mean leaf angle until reaching 20 m, above which mean leaf angle was *c.* 75°. Mean leaf angle in Costa Rica and Virginia forest stands similarly increased with height, with an understory mean of 35° and a canopy mean of 75°. At the tall mangrove site, mean leaf angle decreased with height from 0 to 10 m, above which the mean leaf angle consistently increased, with a canopy mean leaf angle of *c.* 60°.

The magnitude and distribution of PAVD profiles and total PAI depended on the method and representation of LAD (Fig. 10; Table 2). The single 5° zenith bin captured using the hinge angle method provided a more variable representation of the forest canopy. The linear approximation method had the least stable estimates of PAVD, deviating substantially from other profiling methods. The homogeneous and heterogeneous representation of LAD affected PAVD profile shape and magnitude. The linear approximation method deviated −11.0% to +57.8% from the hinge angle method. Assuming homogeneous LAD resulted in −22.9% to +44.7% deviation, whereas the heterogeneous leaf angle assumption ranged from −17.5% to +62.2%. In general, incorporating more detailed leaf angle information in PAI estimates resulted in an increase in average PAI in comparison with the hinge angle method (9.4% and 24.7% higher for homogeneous and heterogeneous assumptions, respectively).

Net canopy photosynthesis, absorbed PAR, and SIF differed by −3.6% to +24.13% between the hinge angle approach and the two *G*-function approaches (Table 3). The differences varied by site: Virginia had the lowest percentage of difference, whereas Colorado, on average, had the highest. There was no clear

difference between broadleaf and needleleaf sites. In each site, the difference in the simulated photosynthesis rate was usually larger than the difference in APAR and SIF.

## Discussion

The TLSLEAF method is an objective, rapid, and user-friendly method of calculating LAD from single-scan TLS data. TLSLEAF integrates past methods of leaf angle computation (Bailey & Mahaffee, 2017) and leaf-wood classification (Krishna Moorthy *et al.*, 2019) in an accessible, function-based processing framework. Here, we show the method can easily be applied in a range of different forest environments without the need for additional user input. By simplifying the processing steps required for this field-based instrument, we are effectively enabling adoption by nonspecialists with a more ecological focus, as opposed to remote-sensing focus. We believe massive-scale processing of TLS data with TLSLEAF will inform global ecological hypotheses, ecosystem modeling, and remote sensing.

## Benchmarking TLSLEAF

TLSLEAF rapidly processes gridded single-scan mid-resolution (8258 × 3214 grid, 0.768 mrad resolution) TLS data in *c.* 9 min, producing a suite of outputs and ecological parameters, including leaf-wood classified point clouds, native-resolution angular estimates, three-dimensionally explicit voxel normalized leaf angle, LADs, and LAD beta parameters (Fig. 5). Scan resolution will affect processing times, but the most time-consuming component of processing, leaf-wood classification,

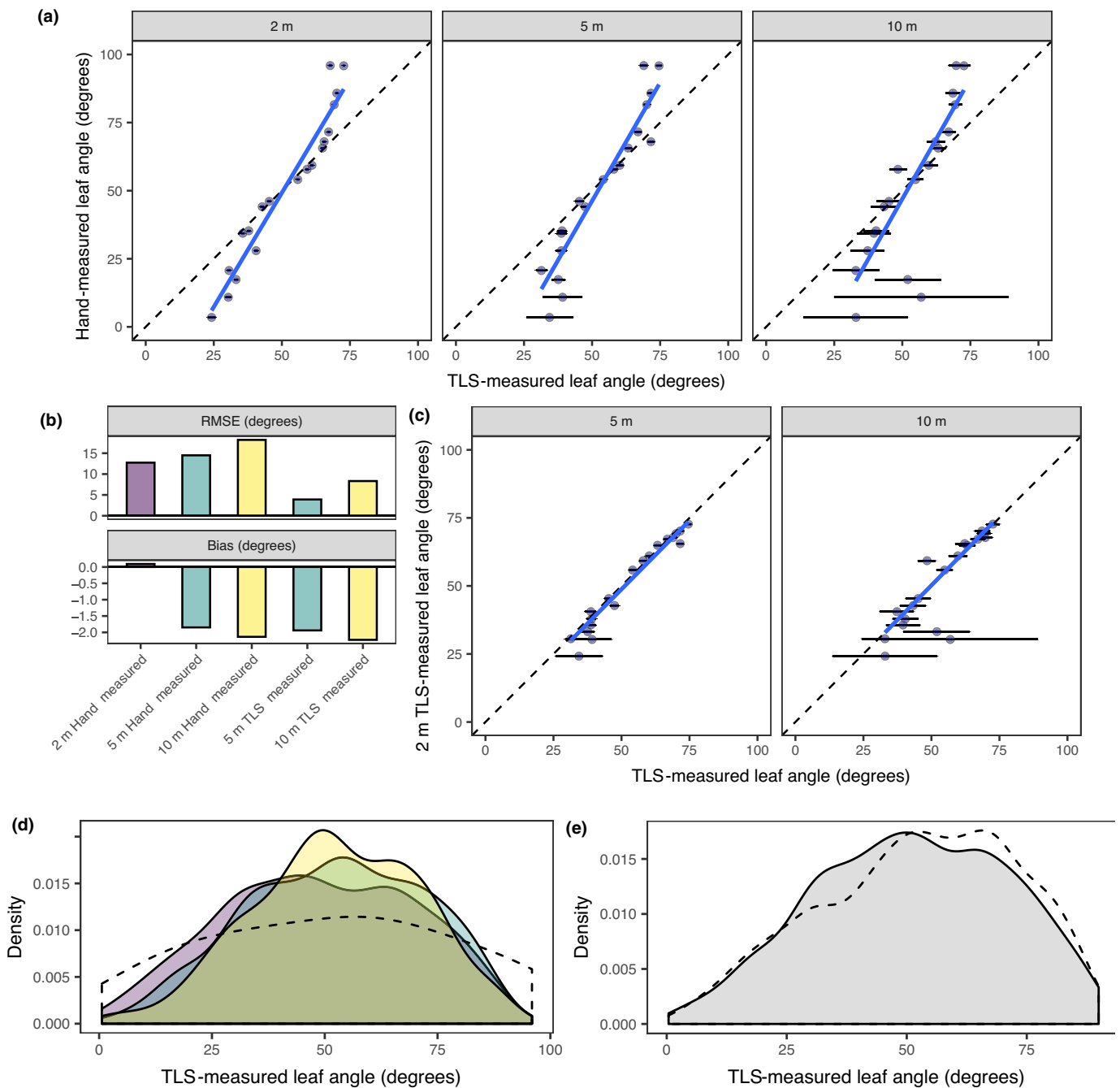


**Fig. 7** Leaf-level validation as a function of distance based on (a) hand-measured and (c) 2 m terrestrial laser scanning (TLS)-measured leaf inclination angle, and (b) RMSE and bias of the validation considering hand-measured and 2 m TLS scans as truth. TLSLeAF estimated leaf angle distributions (c) compared with manual measurements as a function of distance and (b) the effect of aggregation on the area-normalized leaf angle distribution (LAD). (d) Distance – 2 m (purple), 5 m (blue), 10 m (yellow) – has little effect on the TLS-measured LAD and, when aggregated across distances, TLSLeAF provides a statistically similar LAD (Kolmogorov–Smirnov test:  $P = 0.75$ ) to the manual measurements (dotted black line). (e) Treating the 2 m leaf angle measurements as truth (dotted black line) shows minimal effect from aggregating TLS measurements at 10 cm voxel size on the estimated LAD.

will be less impacted by resolution due to a subsampling pre-processing step included in the algorithm. Fig. 5 highlights the rates of each major processing step, but it is worth noting that both steps 2 and 5 include subsampling, reducing the total number of points required for processing in subsequent steps. The current version of TLSLeAF is efficient enough to be applied on a large scale – all output parameters could be

generated for *c.* 1000 TLS scans in less than 1 wk of single-threaded computing time.

### Validating TLSLeAF

TLSLeAF effectively captures broadleaf leaf angle at the sub-leaf scale. The major factors that can affect leaf-level angular



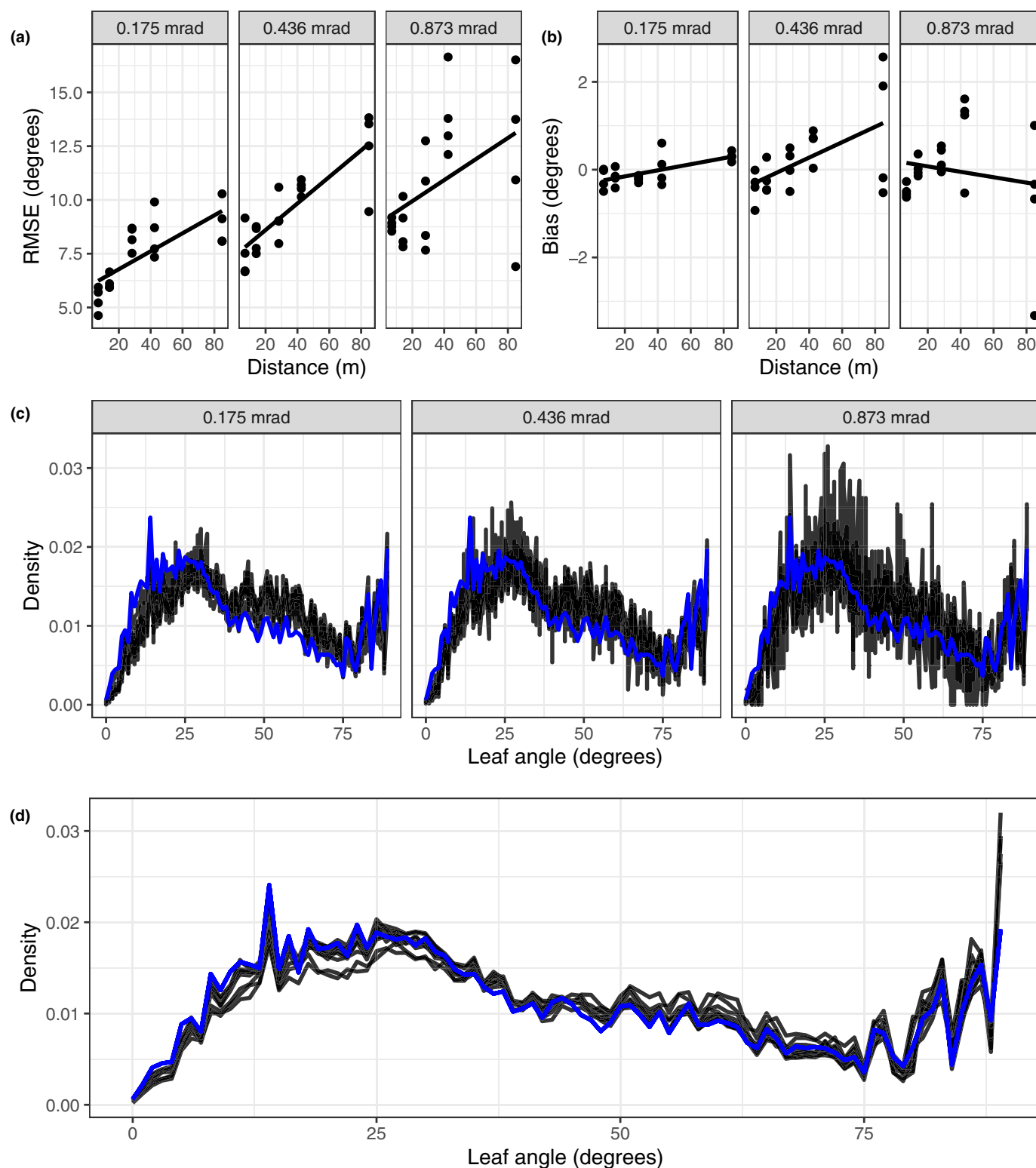


**Fig. 8** Simulation validation for (a–c) single tree and (d) forest scenarios. (a) RMSE and (b) bias increase with distance from tree and with more coarse-resolution scans, with occlusion accounting for a greater proportion of the uncertainty at greater distances. (c) Degraded scan resolution increases variability in the leaf angle distribution (LAD; black) in comparison with the true full-tree LAD (blue), but multiple scans improve confidence, reducing uncertainty from occlusion. (d) In the forest scenario, scan position (black) had little effect on the resulting LAD.

measurements with TLS are scattering angle, scan resolution, distance, and occlusion. Leaf inclination angles closely matching view angle can negatively impact the precision of leaf

measurements due to a reduced number of returns and a high scattering angle, introducing ranging errors. Though edge returns and high scattering angle are filtered with TLSLeAF, it remains a

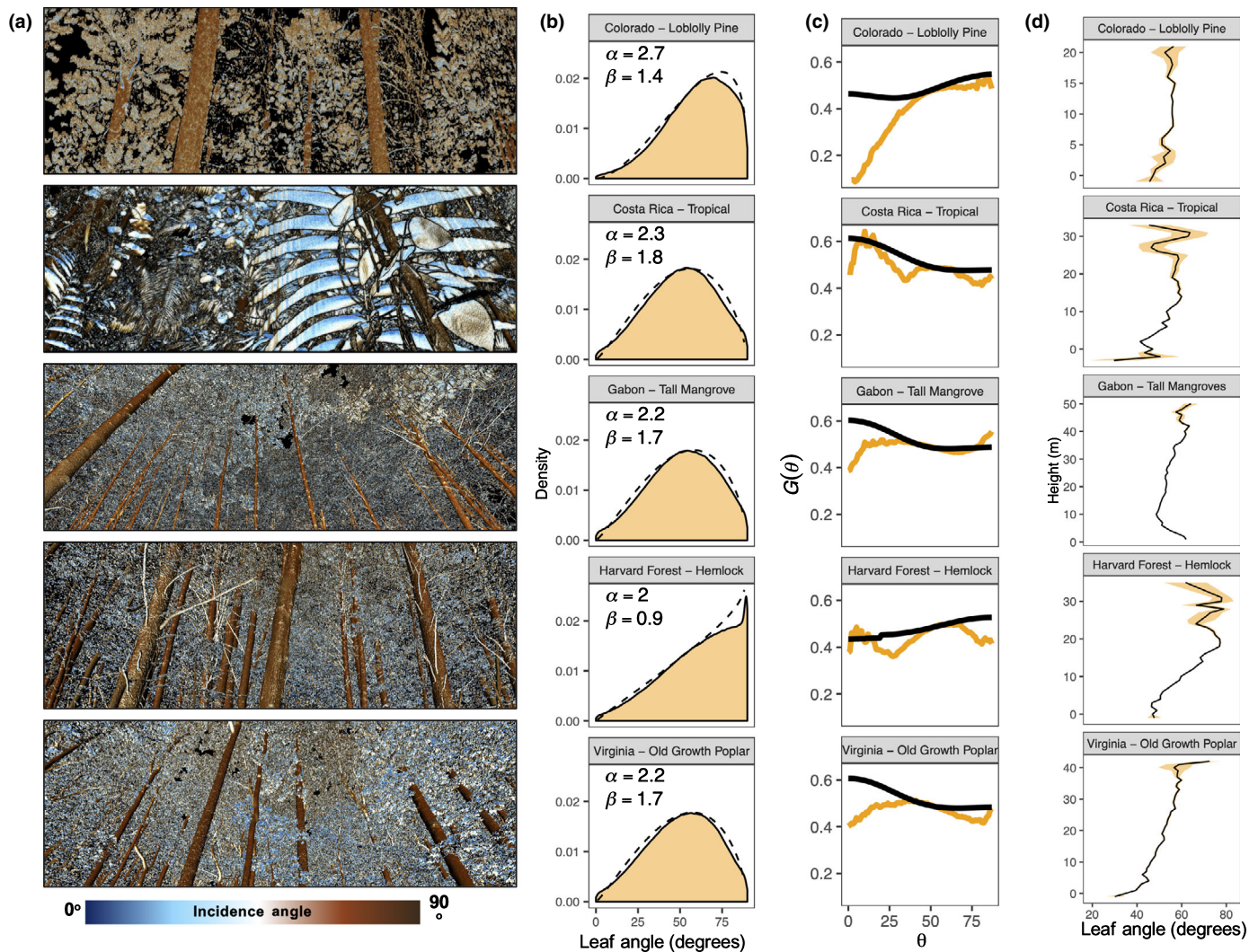


**Fig. 9** The five example forested sites with derived leaf angle parameters (terrestrial laser scan subset area and angles shown in (a)) including (b) leaf angle distributions and associated beta distributions (black dotted lines; parameters shown), (c) random (black) and nonrandom (orange)  $G$ -functions, and (d) vertical distributions of mean leaf angle (black) with 95% confidence intervals (shaded orange).

major technological challenge to effectively reconstruct all leaves in the forest canopy with minimal error. Over the interval evaluated in the laboratory, errors due to distance from the leaf play less of a role in TLSLEAF measurement uncertainty. Though our evaluation of measurement distance included only three distances, we found a *c.*  $0.69^{\circ}$ – $0.88^{\circ}$  increase in RMSE per meter, suggesting – like other TLS-derived variables – distance is most detrimental in taller canopies ( $> 30$  m). Our extension of this analysis into the simulated tree and forest scenarios was consistent, showing increasing RMSE with distance, but also highlighted the role of scan angular resolution and occlusion as important factors affecting LAD reconstruction accuracy. The relative impact of these factors on gridded normal and inclination angle computation is in line with past work (Bailey & Mahaffee, 2017), albeit improved upon, since TLSLEAF automatically classifies and isolates leaves, reducing bias from wood interceptions in LAD estimates (Woodgate *et al.*, 2016; Calders *et al.*, 2018). One clear mitigating strategy for constraining uncertainty in leaf-level angular estimates with TLS is to collect multiple sample

locations per plot or site (as is already typical in TLS sampling; e.g. Wilkes *et al.*, 2017) and limit the returns by distance from the scanner. Multiple scan locations will also improve undersampling in canopy measurements due to occlusion. A systematic evaluation of factors affecting leaf-level angle uncertainty using TLSLEAF will enable appropriate error propagation for derived estimates of PAI and PAVD.

At present, applications of TLSLEAF in needleleaf forests should be considered with caution, as there is no current robust means of validating the angular estimates of needles. The reason for this is both logistical and technical. Even in a laboratory setting, capturing the angle of individual needles is at best cumbersome and at worst inaccurate. A single cluster of needleleaves may contain tens of individuals interspersed and clumped. In short, collecting unbiased hand measurements of needleleaves is not feasible at scale. Instrument limitations are a major factor in the measurement of needleleaf trees. Specifically, LiDAR relies on intercepting a solid surface to capture a reliable range distance. As the intercepted surface become more porous the range



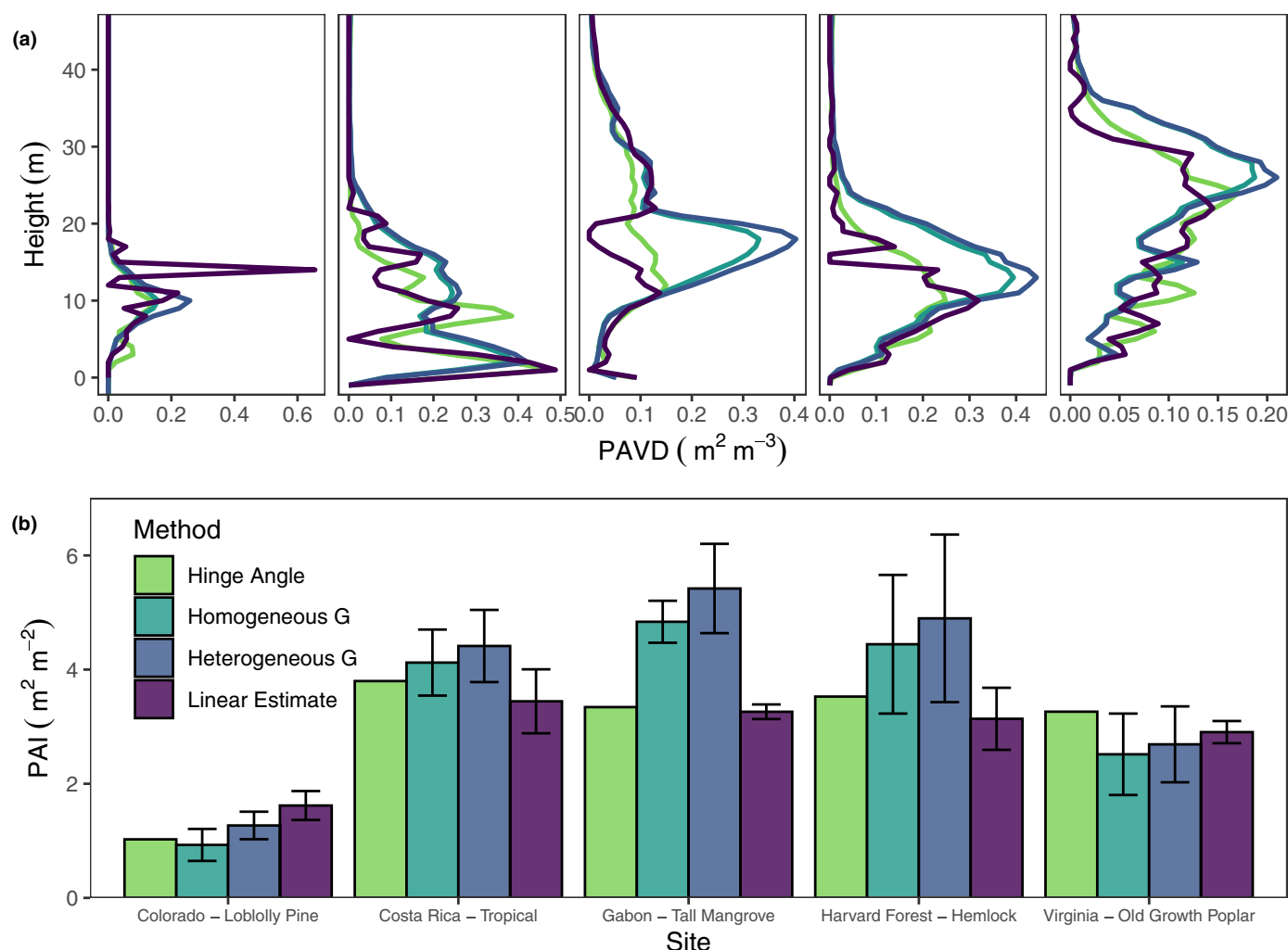


**Fig. 10** Impacts from varying representations of leaf angle distribution captured with TLSLeAF on (a) plant area vegetation density (PAVD) and (b) plant area index (PAI) for the five study sites. We compare the methods of hinge angle and heterogeneous and homogeneous leaf angle distributions for five forested sites. Error bars show the 95% confidence interval of mean PAI derived across all zenith angles (excluding the hinge angle method, since it is derived from a single zenith bin).

**Table 2** Summary statistics for plant area index (PAI) deviation ( $\text{m}^2 \text{m}^{-2}$ ) from typical hinge angle estimates.

| Method          | Mean | %    | SD  | %    | Min  | %     | Max | %    |
|-----------------|------|------|-----|------|------|-------|-----|------|
| Hinge angle     | —    | —    | —   | —    | —    | —     | —   | —    |
| Homogeneous G   | 0.4  | 9.4  | 0.9 | 27.0 | −0.8 | −22.9 | 1.5 | 44.7 |
| Heterogeneous G | 0.8  | 24.7 | 1.0 | 29.4 | −0.6 | −17.5 | 2.1 | 62.2 |
| Linear estimate | −0.1 | 4.8  | 0.4 | 29.8 | −0.4 | −11.0 | 0.6 | 57.8 |

The commonly used hinge angle method was used as a baseline for calculating PAI deviation.

estimates become more uncertain (Stovall *et al.*, 2017). Soft targets, such as needles, are a ‘worst-case scenario’, in that the individual objects are substantially smaller than the LiDAR beam diameter at virtually all distances. Though a range estimate is returned, the orientation of objects smaller than the beam diameter cannot be captured. As such, in needleleaf forests, the majority

of LiDAR returns are from the exterior portion of needle clusters. The same is true of angular estimates – angles are more likely to represent the angular distribution of needle clusters. Until major technological advances in TLS technology occur (e.g. extremely low beam divergence and/or low-noise range estimates), TLS-based LAD estimates in needleleaf forests will be most representative of the surface curvature of needles as opposed to the true angular distribution of needles.

TLS measurements of leaf angle are unique, in that they measure minute differences in leaf curvature unable to be captured with a single manual or photo-based measurement. Fig. 6 highlights how TLS-based angular measurements capture a wider range of angles within a single leaf than the more subjective single manual leaf angle measurement. Given the subjective nature of hand measurements on curved leaves, we suspect the angular estimates in the validation data set were more likely biased than the TLS measurements (Fig. 7). In this way, manual measurements (e.g. Hutchison *et al.*, 1986) and photographic estimates (Chianucci *et al.*, 2018), which assume planar leaf surfaces in the

**Table 3** Summary statistics for mSCOPE simulations with leaf area index profiles estimated with three different methods.

| Site | Hinge angle |         |        | Homogeneous G |                 |                | Heterogeneous G |                 |                 |
|------|-------------|---------|--------|---------------|-----------------|----------------|-----------------|-----------------|-----------------|
|      | Atot        | APAR    | SIF    | Atot          | APAR            | SIF            | Atot            | APAR            | SIF             |
| HF   | 27.92       | 1154.26 | 0.3943 | 30.6 (9.60%)  | 1232.88 (6.81%) | 0.4076 (3.37%) | 30.95 (10.85%)  | 1241.63 (7.57%) | 0.4088 (3.68%)  |
| GA   | 28.01       | 1163    | 0.3996 | 30.28 (8.10%) | 1225.86 (5.40%) | 0.4076 (2.00%) | 30.78 (9.89%)   | 1238.97 (6.53%) | 0.4093 (2.43%)  |
| VA   | 27.79       | 1156.75 | 0.3988 | 28.02 (0.82%) | 1163.17 (0.56%) | 0.3996 (0.20%) | 28.51 (2.59%)   | 1176.99 (1.75%) | 0.4014 (0.65%)  |
| CR   | 28.95       | 1189.31 | 0.403  | 30.18 (4.24%) | 1223.29 (2.86%) | 0.4073 (1.07%) | 30.5 (5.35%)    | 1231.86 (3.58%) | 0.4084 (1.34%)  |
| CO   | 13.59       | 713.24  | 0.2998 | 13.1 (−3.6%)  | 694.76 (−2.59%) | 0.294 (−1.93%) | 16.87 (24.13%)  | 828.31 (16.13%) | 0.3336 (11.27%) |

HF, Harvard Forest; GA, Gabon; VA, Virginia; CR, Costa Rica; CO, Colorado; Atot, net canopy photosynthesis ( $\mu\text{mol m}^{-2} \text{s}^{-1}$ ); APAR, adsorbed photosynthetically active radiation ( $\mu\text{mol m}^{-2} \text{s}^{-1}$ ); SIF, top-of-canopy hemispherical solar-induced Chl fluorescence (650–800 nm,  $\text{W m}^{-2}$ ). The relative difference between the method and the first method (hinge angle) are shown in parentheses.

canopy, potentially obscure the distribution of angles that truly exist in vegetated canopies. As such, the multiple leaf angle estimates per leaf from TLSLEAF provide a more precise representation of LAD. Implementing LADs with the full angular distribution of sub-leaf curvature will provide more realistic estimates of canopy light interception, further refining radiative transfer modeling, with applications to remote sensing and process-based photosynthesis models.

LADs are extremely difficult to measure, with each method – manual, photo, TLS – having clear benefits and drawbacks. The traditional manual methods (Hutchison *et al.*, 1986) provide the confidence of physically seeing the leaf, but, as with any manual method, are susceptible to user bias and error. Photo-based methods (Chianucci *et al.*, 2018) improve upon traditional methods by providing a method less dependent on the user. Recently, unoccupied aerial vehicles (UAVs) have been used to measure LADs in the canopy using the photo-based method (McNeil *et al.*, 2016). Accessing the canopy with UAVs is a major step toward improving canopy LADs, but occlusion of the interior canopy remains a major challenge with this method. TLS is the only method that rapidly captures reliable leaf angle measurements throughout the canopy, providing less biased and less user-dependent measurements. At sites with flux towers, TLS can be installed for high-frequency canopy measurements of LAD. Cost remains the greatest initial hurdle with TLS, but instruments continue to become more affordable. Now, with ‘plug-and-play’ software such as TLSLEAF, TLS measurements of canopy LAD and PAVD can be adopted by nonspecialists, further increasing accessibility to the ecological community.

### Applications of TLSLEAF in diverse forest types

TLSLEAF can be directly applied to a diverse array of forest ecosystems to retrieve leaf angle estimates for improved site-level and ecosystem-level LADs. Here, we provide five example sites to illustrate the sensitivity of TLSLEAF to different forest types. Broadleaf temperate and tropical systems tended to have planophile LADs, whereas needleleaf systems were more spherical to erectophile. Across systems, a random LAD assumption produces a smooth *G*-function, while capturing the nonrandom aspects of LAD indicates that substantial spatial variation exists in the *G*-function, invalidating the common assumption that

LAD is randomly distributed within the canopy. By capturing the vertical dimension of leaf angle, we found mean leaf angle decreased with height in tropical and temperate broadleaf systems, highlighting the importance of quantifying LADs at different canopy strata. Vertical variations in leaf angle are critical to the understanding of canopy light absorption and leaf trait profiles (Niinemets *et al.*, 2015). With TLSLEAF, we can now directly address the nonrandom, spatially variable nature of leaf angle, improving the characterization of leaf angle and leaf area across forested ecosystems.

By relying on fewer assumptions of canopy characteristics through direct measurements of leaf angle we are able to capture PAVD and PAI more precisely. Compared with the typical gap-fraction-based PAI estimates, incorporating leaf angle measurements at the scale of a single TLS scan can increase PAI by *c.* 62% (mangrove). We found the hinge angle and linear estimation methods proposed by Jupp *et al.* (2008) produced highly variable foliage profiles in comparison with those multiangular methods incorporating leaf angle measurements. An added benefit of the TLSLEAF method is that variation in canopy structure is more effectively captured across view inclination angles using both random and nonrandom LAD assumptions. In comparison, the hinge angle method relies on scaling each relative PAVD from a single angular range, whereas the linear estimation derives variation from the slope fit of the linear model (Jupp *et al.*, 2008).

We showed that the impact of different vertical profiles of LAI cannot be ignored: in some cases, the difference has resulted in a difference in net photosynthesis by > 20%. Though the range of differences in total photosynthesis (Atot) under different representations of leaf area profiles (2.6–24.1%) may seem small, this upward shift is within or exceeding the uncertainty in global primary production: 8 Pg C yr<sup>−1</sup> out of 123 Pg C yr<sup>−1</sup> (*c.* 6%; Beer *et al.*, 2010). The full impact of including vertical profile of leaf angle in models remains to be studied. To our knowledge, there is no radiative transfer model (that can also simulate photosynthesis) accounting for the vertical variation in leaf angle. mSCOPE only uses one LAD for the entire canopy, and from our results we provide evidence of vertical variation in leaf angle. Thus, a critical need for future radiative transfer models is the additional capacity to directly accept data generated by TLS.

Given the ubiquitous use of PAI as a key ecosystem variable, improving LADs in different forest ecosystems with TLSLEAF has major implications for global ecological hypotheses, ecosystem modeling, and remote sensing. Large-scale leaf angle studies are absent from the literature since objective and efficient means of measuring this variable were unavailable. Now, TLS-based leaf angle measurements will enable studies of leaf angle and its variation with seasonal change, abiotic constraints, and competition, among other things. With an easy and automatic method of capturing leaf angle, these new measurements can be linked to biome or plant functional type for use in functional ecological models for refined photosynthetic rates, competition, ecosystem flux, and light interception. For example, more accurate and independent angular estimates of canopy PAVD through directly measured  $G$ -functions will improve estimates of canopy complexity – a strong predictor of ecosystem biodiversity (Walter *et al.*, 2021). Likewise, more direct characterization of leaf angle will directly impact remotely sensed estimates of PAI, from ground-based (hemispherical photography or TLS) to air and space-borne (multispectral optical; LiDAR) sensors (Tang *et al.*, 2012; Hancock *et al.*, 2019; Dubayah *et al.*, 2020). From a low or near-nadir view angle, accurate estimates of the  $G$ -function are key since they act as a highly sensitive nonlinear scalar on estimates of PAI. Using Eqn 8, we found that the  $k$  coefficient ( $\cos(\theta)/G(\theta)$ ) at a nadir view angle nonlinearly varies between 1 and 20, with the most sensitive range occurring with low  $G$ -function values. A number of the forest types evaluated here had major differences in the  $G$ -function at low view angles, depending on the means of characterizing LAD – further motivation for incorporating TLS LADs into remote-sensing estimates of PAI moving forward.

TLSLEAF is an efficient open-source processing framework that automatically derives LADs from single-scan TLS data. We anticipate further algorithm improvements may come with more robust wood–leaf classifiers in different ecosystems, smoothing of local normal calculations, and individual leaf isolation, but the current algorithm is automatic and effective. We also note laser scanner quality (e.g. signal-to-noise ratio) will improve LAD estimates. To our knowledge, this approach is now the fastest and most user-accessible means of calculating leaf angle and LADs (Fig. 5). As such, TLSLEAF is poised to enable widespread automated scan-level processing of available TLS data, relevant for addressing, among other things, ecological theory, remote sensing, and ecosystem modeling.




## Acknowledgements

AELS is funded by the NASA Postdoctoral Program Fellowship and the National Aeronautics and Space Administration (grant 80NSSC17K0110). XY is funded by National Science Foundation through the Division of Integrative Organismal Systems (grant 2005574) and the National Aeronautics and Space Administration (grant 80NSSC17K0110). LF and AELS were funded by the NASA Carbon Monitoring System Program Project ‘Estimating total ecosystem carbon in blue carbon and tropical peatland ecosystems’ (16-CMS16-0073).

## Author contributions

AELS and XY conceived the research. AELS developed the TLSLEAF algorithm. XY conducted the mSCOPE model simulations. BM conducted the laboratory-based validation experiment. AS conducted all analyses. AELS, XY and LF edited the manuscript.

## ORCID

Lola Fatoyinbo  <https://orcid.org/0000-0002-1130-6748>  
Atticus E. L. Stovall  <https://orcid.org/0000-0001-9512-3318>  
Xi Yang  <https://orcid.org/0000-0002-5095-6735>

## Data availability

TLSLEAF is freely available online (<https://github.com/aestovall/TLSLeAF>). Site data sets and simulation data presented will be made available upon request to the corresponding author.

## References

- Badino H, Huber D, Park Y, Kanade T. 2011. Fast and accurate computation of surface normals from range images. In: *2011 IEEE International Conference on Robotics and Automation*. Piscataway, NJ, USA: IEEE, 3084–3091.
- Bailey BN, Mahaffee WF. 2017. Rapid measurement of the three-dimensional distribution of leaf orientation and the leaf angle probability density function using terrestrial LiDAR scanning. *Remote Sensing of Environment* **194**: 63–76.
- Beer C, Reichstein M, Tomelleri E, Ciais P, Jung M, Carvalhais N, Rodenbeck C, Arain MA, Baldocchi D, Bonan GB *et al.* 2010. Terrestrial gross carbon dioxide uptake: global distribution and covariation with climate. *Science* **329**: 834–838.
- Brodu N, Lague D. 2012. 3D terrestrial LiDAR data classification of complex natural scenes using a multi-scale dimensionality criterion: applications in geomorphology. *ISPRS Journal of Photogrammetry and Remote Sensing* **68**: 121–134.
- Calders K, Adams J, Armston J, Bartholomeus H, Bauwens S, Bentley LP, Chave J, Danson FM, Demol M, Disney M *et al.* 2020. Terrestrial laser scanning in forest ecology: expanding the horizon. *Remote Sensing of Environment* **251**: e112102.
- Calders K, Origo N, Disney M, Nightingale J, Woodgate W, Armston J, Lewis P. 2018. Variability and bias in active and passive ground-based measurements of effective plant, wood and leaf area index. *Agricultural and Forest Meteorology* **252**: 231–240.
- Chianucci F, Pisek J, Raabe K, Marchino L, Ferrara C, Corona P. 2018. A dataset of leaf inclination angles for temperate and boreal broadleaf woody species. *Annals of Forest Science* **75**: e50.
- CloudCompare. 2020. *CLOUDCOMPARE: 3D point cloud and mesh processing software*. [WWW document] URL <https://www.danielgm.net/cc/> [accessed 4 August 2020].
- Darwin C. 1881. *The power of movement in plants*. New York, NY, USA: D. Appleton.
- Disney M. 2019. Terrestrial LiDAR: a three-dimensional revolution in how we look at trees. *New Phytologist* **222**: 1736–1741.
- Disney M, Burt A, Calders K, Schaaf C, Stovall A. 2019. Innovations in ground and airborne technologies as reference and for training and validation: terrestrial laser scanning (TLS). *Surveys in Geophysics* **40**: 937–958.
- Dubayah R, Blair JB, Goetz S, Fatoyinbo L, Hansen M, Healey S, Hofton M, Hurtt G, Kellner J, Luthcke S *et al.* 2020. The global ecosystem dynamics investigation: high-resolution laser ranging of the Earth's forests and topography. *Science of Remote Sensing* **1**: e100002.
- Ehleringer J, Forseth I. 1980. Solar tracking by plants. *Science* **210**: 1094–1098.



- Frankenberg C, Fisher JB, Worden J, Badgley G, Saatchi SS, Lee J-E, Toon GC, Butz A, Jung M, Kuze A *et al.* 2011. New global observations of the terrestrial carbon cycle from GOSAT: patterns of plant fluorescence with gross primary productivity. *Geophysical Research Letters* 38: L17706.
- Givnish TJ. 2020. The adaptive geometry of trees revisited. *The American Naturalist* 195: 935–947.
- Hancock S, Armston J, Hofton M, Sun X, Tang H, Duncanson LI, Kellner JR, Dubayah R. 2019. The GEDI simulator: a large-footprint waveform LiDAR simulator for calibration and validation of spaceborne missions. *Earth and Space Science* 6: 294–310.
- Horn HS. 1971. *The adaptive geometry of trees*. Princeton, NJ, USA: Princeton University Press.
- Hosoi F, Omasa K. 2015. Estimating leaf inclination angle distribution of broad-leaved trees in each part of the canopies by a high-resolution portable scanning LiDAR. *Journal of Agricultural Meteorology* 71: 136–141.
- Hutchison BA, Matt DR, McMillen RT, Gross LJ, Tajchman SJ, Norman JM. 1986. The architecture of a deciduous forest canopy in eastern Tennessee, U.S.A. *The Journal of Ecology* 74: 635–646.
- Jupp DLB, Culvenor DS, Lovell JL, Newnham GJ, Strahler AH, Woodcock CE. 2008. Estimating forest LAI profiles and structural parameters using a ground-based laser called 'Echidna®'. *Tree Physiology* 29: 171–181.
- Kao W-Y, Forseth IN. 1992. Diurnal leaf movement, chlorophyll fluorescence and carbon assimilation in soybean grown under different nitrogen and water availabilities. *Plant, Cell & Environment* 15: 703–710.
- Krishna Moorthy SM, Calders K, Vicari MB, Verbeek H. 2019. Improved supervised learning-based approach for leaf and wood classification from LiDAR point clouds of forests. *IEEE Transactions on Geoscience and Remote Sensing* 58: 3057–3070.
- Lau A, Calders K, Bartholomeus H, Martius C, Raunonen P, Herold M, Vicari M, Sukhdeo H, Singh J, Goodman RC. 2019. Tree biomass equations from terrestrial LiDAR: a case study in Guyana. *Forests* 10: e527.
- Lawrence DM, Fisher RA, Koven CD, Oleson KW, Swenson SC, Bonan G, Collier N, Ghimire B, van Kampenhou L, Kennedy D *et al.* 2019. The Community Land Model version 5: description of new features, benchmarking, and impact of forcing uncertainty. *Journal of Advances in Modeling Earth Systems* 11: 4245–4287.
- MacArthur RH, Horn HS. 1969. Foliage profile by vertical measurements. *Ecology* 50: 802–804.
- Magney TS, Frankenberg C, Fisher JB, Sun Y, North GB, Davis TS, Kornfeld A, Siebke K. 2017. Connecting active to passive fluorescence with photosynthesis: a method for evaluating remote sensing measurements of Chl fluorescence. *New Phytologist* 215: 1594–1608.
- McNeil BE, Pisek J, Lepisk H, Flamenco EA. 2016. Measuring leaf angle distribution in broadleaf canopies using UAVs. *Agricultural and Forest Meteorology* 218–219: 204–208.
- Momo Takoudjou S, Ploton P, Sonké B, Hackenberg J, Griffon S, Coligny F, Kamdem NG, Libalah M, Mofack GII, Le Moguédec G *et al.* 2017. Using terrestrial laser scanning data to estimate large tropical trees biomass and calibrate allometric models: a comparison with traditional destructive approach. *Methods in Ecology and Evolution* 9: 905–916.
- Myneni R. 1986. Canopy architecture, irradiance distribution on leaf surfaces and consequent photosynthetic efficiencies in heterogeneous plant canopies. Part 1. Theoretical considerations. *Agricultural and Forest Meteorology* 37: 189–204.
- Niinemets Ü, Keenan TF, Hallik L. 2015. A worldwide analysis of within-canopy variations in leaf structural, chemical and physiological traits across plant functional types. *New Phytologist* 205: 973–993.
- Posada JM, Lechowicz MJ, Kitajima K. 2009. Optimal photosynthetic use of light by tropical tree crowns achieved by adjustment of individual leaf angles and nitrogen content. *Annals of Botany* 103: 795–805.
- R Core Team. 2019. *R: a language and environment for statistical computing*, v.3.6.2. Vienna, Austria: R Foundation for Statistical Computing.
- Roussel J-R, Auty D, Coops NC, Tompalski P, Goodbody TRH, Sánchez Meador A, Bourdon J-F, de Boissieu F, Achim A. 2020. LiDR: an R package for analysis of airborne laser scanning (ALS) data. *Remote Sensing of Environment* 251: e112061.
- Stovall AEL, Anderson-Teixeira KJ, Shugart HH. 2018. Assessing terrestrial laser scanning for developing non-destructive biomass allometry. *Forest Ecology and Management* 427: 217–229.
- Stovall AEL, Shugart HH. 2018. Improved biomass calibration and validation with terrestrial LiDAR: implications for future LiDAR and SAR missions. *IEEE Journal of Selected Topics in Applied Earth Observations and Remote Sensing* 11: 3527–3537.
- Stovall AEL, Vorster AG, Anderson RS, Evangelista PH, Shugart HH. 2017. Non-destructive aboveground biomass estimation of coniferous trees using terrestrial LiDAR. *Remote Sensing of Environment* 200: 31–42.
- Tang H, Dubayah R, Swatantran A, Hofton M, Sheldon S, Clark DB, Blair B. 2012. Retrieval of vertical LAI profiles over tropical rain forests using waveform LiDAR at La Selva, Costa Rica. *Remote Sensing of Environment* 124: 242–250.
- van der Tol C, Verhoef W, Timmermans J, Verhoef A, Su Z. 2009. An integrated model of soil-canopy spectral radiances, photosynthesis, fluorescence, temperature and energy balance. *Biogeosciences* 6: 3109–3129.
- Verrelst J, Rivera JP, van der Tol C, Magnani F, Mohammed G, Moreno J. 2015. Global sensitivity analysis of the SCOPE model: what drives simulated canopy-leaving sun-induced fluorescence? *Remote Sensing of Environment* 166: 8–21.
- Vicari MB, Pisek J, Disney M. 2019. New estimates of leaf angle distribution from terrestrial LiDAR: comparison with measured and modelled estimates from nine broadleaf tree species. *Agricultural and Forest Meteorology* 264: 322–333.
- Walter JA, Stovall AEL, Atkins JW. 2021. Vegetation structural complexity and biodiversity in the Great Smoky Mountains. *Ecosphere* 12: e03390.
- Wilkes P, Lau A, Disney M, Calders K, Burt A, Gonzalez de Tanago J, Bartholomeus H, Brede B, Herold M. 2017. Data acquisition considerations for terrestrial laser scanning of forest plots. *Remote Sensing of Environment* 196: 140–153.
- Wilson JW. 1960. Inclined point quadrats. *New Phytologist* 59: 1–7.
- Woodgate W, Armston JD, Disney M, Jones SD, Suarez L, Hill MJ, Wilkes P, Soto-Berelov M. 2016. Quantifying the impact of woody material on leaf area index estimation from hemispherical photography using 3D canopy simulations. *Agricultural and Forest Meteorology* 226–227: 1–12.
- Yang P, Verhoef W, van der Tol C. 2017. The mSCOPE model: a simple adaptation to the SCOPE model to describe reflectance, fluorescence and photosynthesis of vertically heterogeneous canopies. *Remote Sensing of Environment* 201: 1–11.
- Yang X, Tang J, Mustard JF, Lee J-E, Rossini M, Joiner J, Munger JW, Kornfeld A, Richardson AD. 2015. Solar-induced chlorophyll fluorescence that correlates with canopy photosynthesis on diurnal and seasonal scales in a temperate deciduous forest: fluorescence and photosynthesis. *Geophysical Research Letters* 42: 2977–2987.

## Supporting Information

Additional Supporting Information may be found online in the Supporting Information section at the end of the article.

**Fig. S1** Visualization of simulation validation concept and simulation output.

**Fig. S2** Minimum measurable leaf size for a given distance measurement at four scattering angles and assuming a 0.768 mrad angular resolution.

**Fig. S3** LAD sensitivity to voxel size ranging from 2 cm to 1 m for the mixed deciduous forest site in Virginia, USA.

**Notes S1** TLS acquisitions.

**Notes S2** Simulation validation.

**Notes S3** Sensitivity to TLS parameters and voxel resolution.

Please note: Wiley Blackwell are not responsible for the content or functionality of any Supporting Information supplied by the

authors. Any queries (other than missing material) should be directed to the *New Phytologist* Central Office.